# Recoil Inversion in the Photodissociation of Carbonyl Sulfide near 234 nm

Dimitris Sofikitis,[1,2,*] Jaime Suarez,[3] Johan A. Schmidt,[4] T. Peter Rakitzis,[2,5] Stavros C. Farantos,[2,6] and Maurice H. M. Janssen[1,†]

[1]LaserLaB Amsterdam, Vrije Universiteit, de Boelelaan 1081, 1081 HV Amsterdam, Netherlands
[2]Institute of Electronic Structure and Laser, Foundation for Research and Technology–Hellas, 71110 Heraklion-Crete, Greece
[3]Departamento de Qumica, Modulo 13, Universidad Autonoma de Madrid, Cantoblanco 28049, Madrid, Spain
[4]Department of Chemistry, University of Copenhagen, Universitetsparken 5, DK-2100 Copenhagen Ø, Denmark
[5]Department of Physics, University of Crete, 70013 Heraklion-Crete, Greece
[6]Department of Chemistry, University of Crete, 70013 Heraklion-Crete, Greece

(Received 28 September 2016; published 20 June 2017)

We report the observation of recoil inversion of the CO ($v = 0, J_{CO} = 66$) state in the UV dissociation of lab-frame oriented carbonyl sulfide (OCS). This state is ejected in the opposite direction with respect to all other ($> 30$) states and in absence of any OCS rotation, thus resulting in spatial filtering of this particular high-$J$ rovibrational state. This inversion is caused by resonances occurring in shallow local minima of the molecular potential, which bring the sulfur closer to the oxygen than the carbon atom, and is a striking example where such subtleties severely modify the photofragment trajectories. The resonant behavior is observed only in the photofragment trajectories and not in their population, showing that stereodynamic measurements from oriented molecules offer an indispensable probe for exploring energy landscapes.

DOI: 10.1103/PhysRevLett.118.253001

Photodissociation of small molecules is a relatively straightforward process connecting the reactants and products of a reaction, and this is why photodissociation studies provide an excellent starting point for understanding the nature of the various chemical bonds [1], as well as for the (coherent) control of reactions [2,3].

Modern spectroscopic techniques, such as ion imaging [4], velocity map imaging (VMI) [5] or Rydberg tagging [6], allow advanced studies of the geometrical aspects of dissociation, which can now be observed directly rather than being inferred by the study of single-dimensional, wavelength-dependent spectra. Such studies demonstrate that dissociation reactions are often the result of complicated underlying mechanisms [7–9], as, for example, the coherent excitation to multiple dissociative states [10–12] or the roaming mechanism in the dissociation of formaldehyde and other small molecules [13,14].

An even more detailed picture of the stereodynamical aspects of photodissociation can be extracted by orienting the parent molecules in the lab frame prior to dissociation. Lab-frame orientation, achieved either by static electric [15–19] or optical fields [20–25], can define an initial orientation of the chemical bond in space and avoid the statistical "washing out" of the dissociation geometry caused by the parent molecule free rotation [23,26–32]. Furthermore, a wide variety of spectroscopic tools are constantly being developed that can be used to extract stereodynamical information in dissociation, such as delay line coincidence VMI [33,34] or cold target recoil-ion momentum spectroscopy [35].

When the photodissociation of lab-frame oriented molecules is considered, the photofragment spatial distribution is described through an expansion in Legendre polynomials $P_n$: $I(\theta) \propto 1 + \sum_{i=1}^{4} \beta_i P_i(\cos\theta)$. The odd terms are related to up-down asymmetries, and the even terms are related to parallel-perpendicular asymmetries. In the absence of orientation, all odd terms are zero [10,19,26,27,36–39].

Isolated molecules $A$-$B$ can be oriented in the lab frame, e.g., with $A$ up and $B$ down; after photodissociation, one would expect that the $A$ fragment would recoil upwards and $B$ downwards. Here, we report dissociation experiments of OCS molecules oriented with CO downwards. Surprisingly, for a specific photolysis energy, the highest rotational photofragment state CO ($v = 0$, $J_{CO} = 66$) recoils upwards, in contrast to all other states, $34 \le J_{CO} \le 65$, and in the absence of any OCS rotation. This recoil inversion is observed over a narrow range of photolysis energy, over which the $\beta_1$ and $\beta_2$ parameters are observed to vary strongly in a resonantlike fashion. These variations of the recoil direction are not accompanied by a variation of the particular state intensity and, thus, are detectable only by examination of the angular distribution. We show that this behavior can be explained by the presence of resonances in shallow local minima of the molecular potential which result in the sulfur atom ejected from the side of the oxygen rather than the carbon atom.

In Fig. 1(a), we display an image of $S(^1D_2)$ photofragments produced by OCS dissociation around 42 700 $cm^{-1}$. Here, the orientation field is turned off, so that the parent OCS molecules have random orientation in space. The sulfur ions recoil in several distinct narrow velocity groups, each one corresponding to the production of CO molecules in a different rotational state. This provides an indirect but simultaneous measurement of the velocity distribution of

 

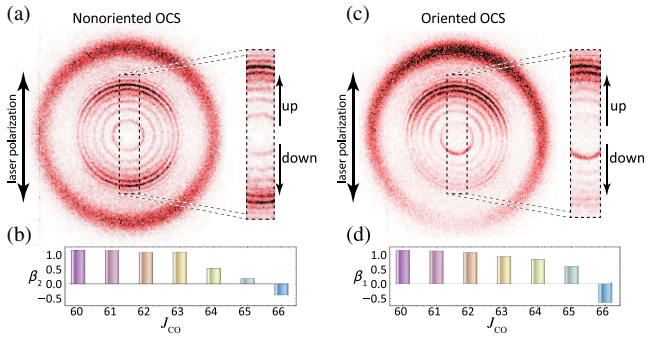


FIG. 1. (a) Sliced image of ionized sulfur atoms produced by the photodissociation of nonoriented OCS molecules at ~42 700 $cm^{-1}$. (b) Values of the $\beta_2$ coefficient for $60 \leq J_{CO} \leq 66$ states, extracted from (a). (c) Same as (a) for the photodissociation of oriented OCS molecules at ~42 700 $cm^{-1}$. The CO fragments move antiparallelly to the detected *S*-atom cofragments. (d) Values of $\beta_1$ coefficient for the states with $60 \leq J_{CO} \leq 66$ extracted from (c).

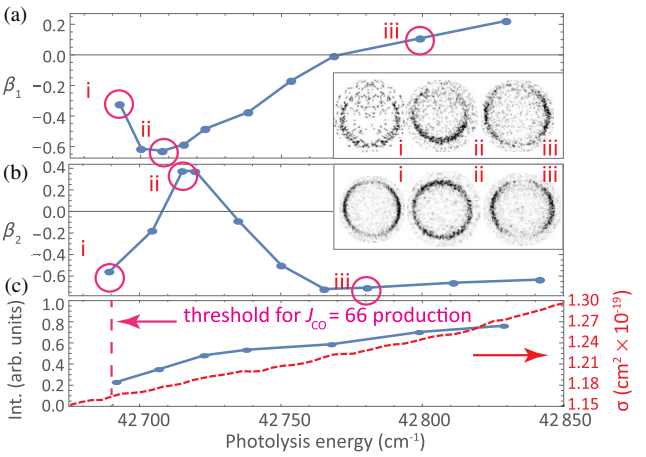


FIG. 2. The $J_{CO} = 66$ state. (a) Dependence of the $\beta_1$ parameter on the photolysis energy, for oriented OCS parent molecules. (Inset) Sliced ion images for three different photolysis energies. (b) Dependence of the $\beta_2$ parameter on the photolysis energy, for nonoriented OCS parent molecules. (Inset) Sliced ion images for three different photolysis energies. (c) Total intensity as a function of the photolysis laser energy. The red dashed line shows the total absorption cross section [40,41].

several molecular states. For our focusing conditions of the VMI lens, we can clearly resolve several rotational states ($J_{CO} = 59$–66). Notice that the sliced image is up-down symmetric, meaning that ions are emitted both upwards and downwards with equal probability within experimental accuracy (see the enlargement of the central slice). The intensity of the fragments is reduced in the plane parallel to the laser propagation (i.e., perpendicular to the laser polarization), reflecting a small contribution from perpendicular dissociation channels.

In Fig. 1(b), we show the $\beta_2$ coefficients for the states associated with $60 \leq J_{CO} \leq 66$ extracted from the image shown in Fig. 1(a). As we see, for $J_{CO} = 60$, the $\beta_2$ coefficient is positive (~1.2). As $J_{CO}$ increases, the value of the $\beta_2$ coefficients gradually decreases with the maximum $J_{CO} = 66$ having a negative value ($\sim -0.4$).

In Fig. 1(c), the study is repeated, with the addition of the electric field used to orient the parent OCS molecules in the lab frame with the sulfur atom up. Surprisingly, the sulfur ions associated with the production of $J_{CO} = 66$ molecules (the smallest, middle circle) end up following the opposite direction with respect to all others. This is illustrated in the expansion of the central slice of the ion image, where we see that the ions associated with the $J_{CO} = 66$ state are moving downwards, while all of the other states are almost exclusively emitted upwards. We stress the fact that the parent OCS molecules have a fixed orientation in space prior to dissociation, while no molecular rotation can be transferred to the OCS molecule by the linearly polarized laser fields.

This recoil inversion observed in Fig. 1(c) is described quantitatively in Fig. 1(d), where we plot the value of the $\beta_1$ coefficients: the $\beta_1$ coefficients are all positive (indicating that the sulfur atoms move upwards), with the exception of the atoms associated with the production of $J_{CO} = 66$ molecules. We consider the ratio between the number of sulfur ions associated with the $J_{CO} = 66$ state that recoil downwards and the sum of the number of sulfur ions associated with all other states, which also recoil downwards. This ratio increases by a factor greater than 20 when the parent OCS molecules are oriented, in comparison to unpolarized OCS molecules.

These counterintuitive dynamics manifest themselves only in a narrow spectral region of ~60 $cm^{-1}$. In Fig. 2(a) we show the dependence of the $\beta_1$ coefficient of the photofragments produced by dissociating *oriented* OCS molecules on the photolysis energy (laser bandwidth < 0.5 $cm^{-1}$). The $\beta_1$ coefficient displays a resonantlike dependence: it has a small negative value at threshold, it reaches its minimum value of $\sim -0.6$ after 20 $cm^{-1}$, and gradually increases with increasing dissociation energy reaching positive values within ~60 $cm^{-1}$. These trends are illustrated by showing three characteristic sliced ion images [inset of Fig. 2(a)], cropped to display only the ions associated with the $J_{CO} = 66$ state. These images correspond to the experimental points (i) below resonance, ~42690 $cm^{-1}$; (ii) on resonance, ~42 715 $cm^{-1}$; and (iii) above resonance, ~42 800 $cm^{-1}$. We see that the ion image shown in (i) has most of its intensity on the lower part (negative $\beta_1$). A few tens of $cm^{-1}$ further, the intensity is much more focused on the lower part (lower $\beta_1$), while, by the time the dissociation energy reaches 42 800 $cm^{-1}$, the value of $\beta_1$ is ~0, its sign has been reversed, and the image is nearly up-down symmetric.

A similar resonant behavior is observed in the case of the photodissociation of *nonoriented* OCS molecules. In Fig. 2(b), we see the dependence of the $\beta_2$ coefficient on the photolysis energy: over a 50 $cm^{-1}$ span, $\beta_2$ starts from a relatively low ($\sim -0.6$) value, rapidly reverses sign reaching ~0.4, and reverses sign again. In the inset of Fig. 2(b), we show three characteristic sliced ion images, again

cropped to display only the sulfur ions associated with the $J_{CO} = 66$ state. These images correspond to the experimental points (i) below resonance, 42 700 $cm^{-1}$; (ii) on resonance, ~42 720 $cm^{-1}$; and (iii) above resonance, ~42 780 $cm^{-1}$. As we see in the inset, the sulfur ion angular distribution changes from having most intensity at the sides (a negative $\beta_2$) to having most intensity up and down (a positive $\beta_2$) and back to having most intensity at the sides. The values of the $\beta_3$ and $\beta_4$ are within error of zero, suggesting that any polarization effects related to orbital angular momentum can be neglected.

We stress that this resonant behavior is observed only in the *angular distribution* of the sulfur ions associated with the production of high $J_{CO} \in [63–66]$ molecules. In Fig. 2(c), we display the integrated intensity of the ions associated with the $J_{CO} = 66$ state: the intensity increases monotonically as a function of the photolysis energy and no rapid variations are observed. The red dashed line shows the total absorption cross section in this area [40] (downloaded from Ref. [41]), where the energy axis has been shifted by ~520 $cm^{-1}$ to account for the vibrational excitation of the parent molecule. The cross section is a relatively smooth function of the energy for the examined range, ~42 700–42 850 $cm^{-1}$. Specifically, the $S(^1D)$ spectra (which correspond to $34 < J_{CO} < 66$ excitation) shows no prominent resonant features in this area, in contrast to the $S(^3P)$ spectra (corresponding to a lower $J_{CO}$), in which some weak features are present at energies that are lower by ~520 $cm^{-1}$ [42].

This recoil inversion is a stereodynamical effect, which requires an intrinsic explanation of the mechanism for the energy transfer to the angular degree of freedom. We demonstrate that the existence of resonances predicted by a periodic orbit analysis and calculated by quantum computations localizes the sulfur atom closer to the oxygen rather than the carbon atom. Additionally, the presence of nonadiabatic coupling between different states results in high torques exerted to CO, and thus in populating high rotational states, which are trapped in the resonances for longer times.

The potential energy surfaces (PESs) which are mainly involved in the dissociation process around 42 700 $cm^{-1}$ are the $A$ and $X$ electronic states, and contour plots are shown with broken lines in Figs. 3(a) and 3(b) and Figs. 3(c) and 3(d), respectively [43–45]. The PESs are plotted in Jacobi coordinates. $R$ is the distance of the sulfur atom from the center of mass of CO, and $\gamma$ the angle between the CO bond length ($r$) and $R$, where $\gamma = 0°$ corresponds to the OC-S configuration, and $\gamma = 180°$ to the S-OC one. In the middle part of the $A$ surface [Fig. 3(a)], there is a local minimum at $(R, r, \gamma) = (4.2\ \text{bohr}, 2.2\ \text{bohr}, 48°)$. Similarly, a metastable minimum is present in the $X$ surface [Fig. 3(c)] at $(R, r, \gamma) = (3.4\ \text{bohr}, 2.3\ \text{bohr}, 85°)$. The $A$ surface is directly accessed by the photolysis laser, which transfers population

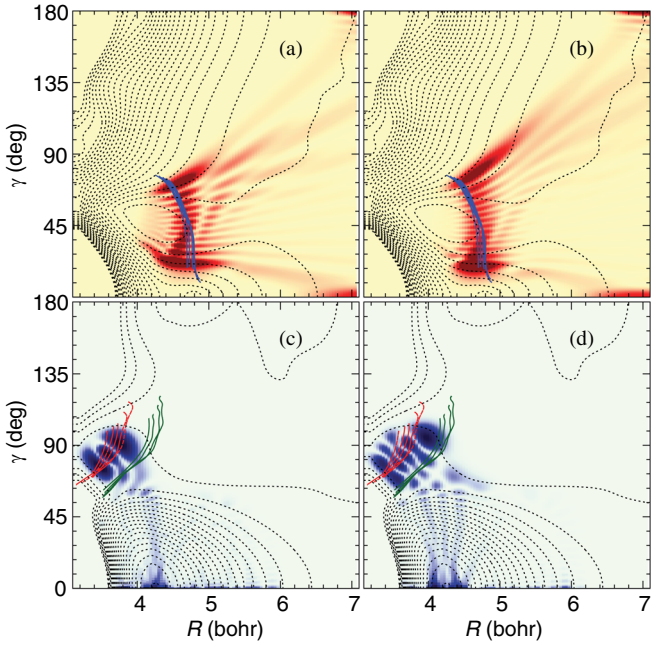


FIG. 3. Contours of the adiabatic PES for the (a),(b) $A$ (brown) and (c),(d) $X$ (cyan) electronic states projected in the $(R, \gamma)$ plane ($r = 2.2$ bohr), with representative periodic orbits and quantum resonance states (see the text). (a) For the $A$ PES, a resonant quantum state is shown at 42 100 $cm^{-1}$ and POs covering [38 000–49 000] $cm^{-1}$. (b) Same as (a) for the resonant quantum state at 42700 $cm^{-1}$. (c) For the $X$ PES, POs covering [33 000–49 000] $cm^{-1}$ (red) and (35 000–48 000) $cm^{-1}$ (green), and a resonant quantum state at 33 715 $cm^{-1}$ alongside the periodic orbits. (d) Same as (c) for a resonant quantum state at 34 430 $cm^{-1}$.

from the (bend vibrationally excited) ground electronic $X$ state. While most of the population proceeds to dissociation directly, a small part is nonadiabatically transferred to the $X$ state, inducing the production of the highest $58 \leq J_{CO} \leq 66$ states [46], as is demonstrated in the following discussion.

The time evolution of the wave packet is studied by employing the grid-time dependent Schrödinger equation (GTDSE) programs [47,48]. Once the wave packet is transferred to the (excited) $A$ surface by the photolysis field, it evolves in time in a nontrivial fashion. The initial wave packet lands in an area close to the linear configuration (S-CO angle, $\gamma \sim 7°$) of the OCS molecule. At later times, while most of the population dissociates in relatively small angles ($\gamma < 60°$), part of the wave packet is trapped near the local minimum shown in Fig. 3(a), accessing localized long-lived resonant states. We depict two such resonant eigenstates at 42 100 $cm^{-1}$ [Fig. 3(a)] and 42 700 $cm^{-1}$ [Fig. 3(b)], both of which exhibit nodal structures that reveal a motion mainly along the $\gamma$ coordinate. The existence of these resonances has been verified by an (independent) periodic orbit (PO) analysis [49], including, in the previous figures, a few periodic orbits in the region of the local minimum of the $A$ state. These unstable POs belong to a family emanated from a

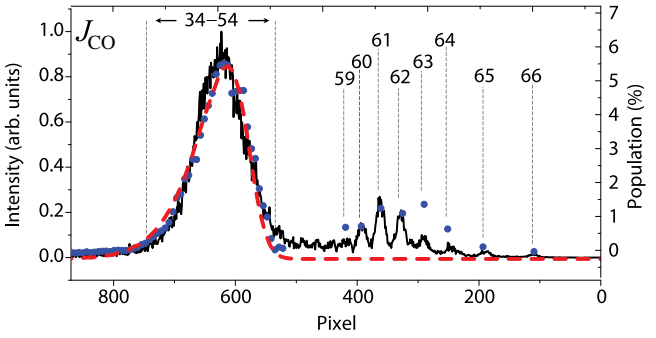


FIG. 4. Angular integration of the ion image shown in Fig. 1(a), depicting the relative intensity of the various $J_{CO}$ states (the black solid line), along with the nonadiabatic (blue dots) populations. The red dashed line is the result of single adiabatic calculations in the $A$ state.

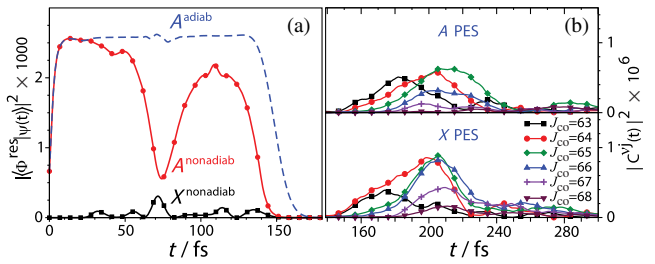


FIG. 5. (a) Time evolution of the overlap integral squared between the excited wave packet and the resonance wave function in the $A$ state shown in Fig. 3(b). (b) The overlap integral of the evolving excitation wave packet in the $A$ and $X$ states with the product states $J_{CO} = 63$–68 wave functions in the nonadiabatic calculations.

center-saddle bifurcation. Their existence and methods to locate them have been discussed before [50].

Most importantly, the resonances found in the excited electronic state are localized in that region of configuration space where the nonadiabatic coupling to the $X$ state is expected to be high [46,51]. Similar classical and quantum calculations on the single adiabatic $X$ PES unveil new resonances which are also related to the recoil inversion. Both resonances depicted in Figs. 3(c) and 3(d), obtained from the GTDSE—as well as the PO analysis—confirm that, in these structures, the sulfur atom is located at small $R$ distances but at larger angles, exploring regions of the phase space where the sulfur atom approaches the oxygen atom. The energies of the two resonances correspond to 33 715 and 34 430 $cm^{-1}$, respectively. At higher energies, close to the experimental ones, the spectrum becomes diffuse, and thus it is difficult to extract eigenfunctions.

Nonadiabatic two state quantum calculations in the internal coordinates $(R, r, \gamma)$ have also been carried out by transforming from an adiabatic to a diabatic representation. The populations of the $J_{CO}$ product states are computed (the blue dots) and are compared with the experimental relative intensities (the black line) in Fig. 4 [52]. The latter are obtained from the angular integration of the ion image presented in Fig. 1(a). By contrast, single adiabatic calculations on the $A$ state yield $J_{CO}$ state contributions only up to 55. These quantum results are in accord with classical surface hopping calculations [46].

The appearance of the two bands in Fig. 4, one covering the range of $34 \leq J_{CO} \leq 54$ and the second $59 \leq J_{CO} \leq 66$, calls for further investigation. In Fig. 5(a), we show the time evolution of the square of the overlap integral between the excited wave packet from the ground to the upper surface and the resonance eigenfunction in the $A$ state shown in Fig. 3(b). Single adiabatic state calculations (the blue broken line) demonstrate that the overlap integral remains almost constant between 10 to 150 fs and is zero after 170 fs. By contrast, we do find population transfer to the ground electronic state in the nonadiabatic calculations. The dip shown in the red curve of Fig. 5(a) (the circles) in the time interval of 50–100 fs occurs in coincidence with the increase of the overlap integral in the ground state (the black line with squares), and it unveils a reflection of the wave packet from the ground back to the excited state. In association with this, Fig. 5(b) depicts the time evolution of the overlap integral of the evolving wave packet with the high $J_{CO} = 63$–68 product states. These states start gaining intensity only after the elapse of ~150 fs, a time which coincides with the diminishing of the overlap of the wave packet with the resonance state [Fig. 3(b)].

The localized quantum resonances along the angular degree of freedom and the production of high $J_{CO}$ states in relatively short times (150 fs) supports dissociation dynamics where the sulfur atom leaves the triatomic molecule from the oxygen side of CO, and thus the recoil inversion observed in the experiment.

In conclusion, we have performed dissociation experiments of lab-frame oriented, as well as nonoriented, OCS molecules around 42700 $cm^{-1}$. We have demonstrated the existence of resonances which bring the sulfur atom closer to the oxygen rather than the carbon atom. These nonadiabatic resonant states can be detected by measuring the photofragment angular distribution for a small range of dissociation energies near the threshold of the $J_{CO} = 66$ state, while not being detectable by any modulation in the population of this state.

Adiabatic and nonadiabatic quantum calculations, in conjunction with a periodic orbit analysis, corroborate the existence of these resonances and illustrate the mechanism for transferring energy from the radial to the angular degree of freedom in association with a population transfer from the $A$ to the ground state [53]. The localization of eigenfunctions to specific degrees of freedom as a result of resonances is a dynamical nonlinear effect found in several small polyatomic molecules [50] but expressed in a different manner for different molecules.

The authors acknowledge the following support: D. S. and T. P. R. from the European Research Council (ERC) Grant TRICEPS (Grant Agreement No. 207542), J. S. from

the ULF-FORTH002179 Laserlab-Europe grant, and J. A. S. from the Carlsberg Foundation postdoctoral fellowship (CF14-0519). The authors are thankful to George McBane for providing the nonadiabatic coupling elements and to Luis Rubio-Lago for useful discussions.

*sofdim@iesl.forth.gr; info@massspecpecd.com
†Present address: MassSpecpecD BV, High Tech Campus University of Twente, Drienerbeeklaan 35, 7522NA Enschede, Netherlands.

[1] R. Schinke, *Photodissociation Dynamics* (Cambridge University Press, Cambridge, England, 1993).
[2] F. F. Crim, J. Phys. Chem. **100**, 12725 (1996).
[3] A. Assionand, T. Baumert, M. Bergt, T. Brixner, B. Kiefer, V. Seyfried, M. Strehle, and G. Gerber, Science **282**, 919 (1998).
[4] D. W. Chandler and P. L. Houston, J. Chem. Phys. **87**, 1445 (1987).
[5] A. T. J. B. Eppink and D. H. Parker, Rev. Sci. Instrum. **68**, 3477 (1997).
[6] X. Yang, Phys. Chem. Chem. Phys. **13**, 8112 (2011).
[7] D. W. Chandler, J. Chem. Phys. **132**, 110901 (2010).
[8] F. A. L. Mauguière, S. C. Farantos, J. Suarez, and R. Schinke, J. Chem. Phys. **134**, 244302 (2011).
[9] M. N. R. Ashfold, B. Cronin, A. L. Devine, R. N. Dixon, and M. G. D. Nix, Science **312**, 1637 (2006).
[10] L. D. A. Siebbeles, M. Glass-Maujean, O. S. Vasyutinskii, J. A. Beswick, and O. Roncero, J. Chem. Phys. **100**, 3610 (1994).
[11] T. P. Rakitzis, S. A. Kandel, A. J. Alexander, Z. H. Kim, and R. N. Zare, Science **281**, 1346 (1998).
[12] T. P. Rakitzis, P. C. Samartzis, and T. N. Kitsopoulos, J. Chem. Phys. **111** 10415 (1999).
[13] D. Townsend, S. A. Lahankar, S. K. Lee, S. D. Chambreau, A. G. Suits, X. Zhang, J. Rheinecker, L. B. Harding, and J. M. Bowman, Science **306**, 1158 (2004).
[14] F. A. L. Mauguière, P. Collins, Z. C. Kramer, B. K. Carpenter, G. S. Ezra, S. C. Farantos, and S. Wiggins, J. Phys. Chem. Lett. **6**, 4123 (2015).
[15] E. W. Kuipers, M. G. Tenner, A. W. Kleyn, and S. Stolte, Nature (London) **334**, 420 (1988).
[16] P. R. Brooks, J. S. McKillop, and H. G. Pippin, Chem. Phys. Lett. **66**, 144 (1979).
[17] H. J. Loesch and A. Remscheid, J. Chem. Phys. **93**, 4779 (1990).
[18] B. Friedrich and D. Herscbach, Nature (London) **353**, 412 (1991).
[19] M. H. M. Janssen, J. W. G. Mastenbroek, and S. Stolte, J. Phys. Chem. **101**, 7605 (1997).
[20] H. Stapelfeldt and T. Seideman, Rev. Mod. Phys. **75**, 543 (2003).
[21] J. P. Heritage, T. K. Gustafson, and C. H. Lin, Phys. Rev. Lett. **34**, 1299 (1975).
[22] F. Rosca-Pruna and M. J. J. Vrakking, Phys. Rev. Lett. **87**, 153902 (2001).
[23] B. Friedrich and D. Herschbach, Phys. Rev. Lett. **74**, 4623 (1995).
[24] W. Kim and P. M. Felker, J. Chem. Phys. **104**, 1147 (1996).
[25] R. Torres, R. de Nalda, and J. P. Marangos, Phys. Rev. A **72**, 023420 (2005).
[26] S. E. Choi and R. B. Bernstein, J. Chem. Phys. **85**, 150 (1986).
[27] R. N. Zare, Chem. Phys. Lett. **156**, 1 (1989).
[28] T. P. Rakitzis, A. van den Brom, and M. H. M. Janssen, Science **303**, 1852 (2004).
[29] A. van den Brom, T. P. Rakitzis, and M. H. M. Janssen, J. Chem. Phys. **121**, 11645 (2004).
[30] T. Seideman, Phys. Rev. Lett. **83**, 4971 (1999).
[31] H. Stapelfeldt, Phys. Scr. T **110**, 132 (2004).
[32] J. G. Underwood, M. Spanner, M. Y. Ivanov, J. Mottershead, B. J. Sussman, and A. Stolow, Phys. Rev. Lett. **90**, 223001 (2003).
[33] A. I. Chichinin, K. H. Gericke, S. Kauczok, and C. Maul, Int. Rev. Phys. Chem. **28**, 607 (2009).
[34] M. M. R. Fanood, N. B. Ram, C. S. Lehmann, I. Powis, and M. H. M. Janssen, Nat. Commun. **6**, 7511 (2015).
[35] J. Ullrich, R. Moshammer, A. Dörn, L. P. H. Schmidt, and H. Schmidt-Böcking, Rep. Prog. Phys. **66**, 1463 (2003).
[36] T. P. Rakitzis, A. J. van den Brom, and M. H. M. Janssen, Chem. Phys. Lett. **372**, 187 (2003).
[37] R. N. Zare, Proc. IEEE **51**, 173 (1963).
[38] R. N. Zare, *Angular Momentum* (Wiley, New York, 1988).
[39] T. Seideman, Chem. Phys. Lett. **253**, 279 (1996).
[40] S. Hattori, S. O. Danielache, M. S. Johnson, J. A. Schmidt, H. G. Kjaergaard, S. Toyoda, Y. Ueno, and N.Yoshida, Atmos. Chem. Phys. **11**, 10293 (2011).
[41] See http://joseba.mpch-mainz.mpg.de/spectral_atlas_data/cross_sections_plots.
[42] B. W. Toulson and C. Murray, J. Phys. Chem. A **120**, 6745 (2016).
[43] J. A. Schmidt, M. S. Johnson, G. C. McBane, and R. Schinke, J. Chem. Phys. **136**, 131101 (2012).
[44] J. A. Schmidt, M. S. Johnson, G. C. McBane, and R. Schinke, J. Chem. Phys. **137**, 054313 (2012).
[45] J. A. Schmidt and J. M. H. Olsen, J. Chem. Phys. **141**, 184310 (2014).
[46] G. C. McBane, J. A. Schmidt, M. S. Johnson, and R. Schinke, J. Chem. Phys. **138**, 094314 (2013).
[47] J. Suarez, S. C. Farantos, S. Stamatiadis, and L. Lathouwers, Comput. Phys. Commun. **180**, 2025 (2009).
[48] J. Suarez, L. Mendez, and I. Rabadan, J. Phys. Chem. Lett. **6**, 72 (2015).
[49] S. C. Farantos, *Nonlinear Hamiltonian Mechanics Applied to Molecular Dynamics: Theory and Computational Methods for Understanding Molecular Spectroscopy and Chemical Reactions* (Springer, New York, 2014).
[50] S. C. Farantos, R. Schinke, H. Guo, and M. Joyeux, Chem. Rev. **109**, 4248 (2009).
[51] T. Suzuki, H. Katayanagi, S. Nanbu, and M. Aoyagi, J. Chem. Phys. **109**, 5778 (1998).
[52] The quantum mechanical populations obtained from a calculation at total energy of 41851 $cm^{-1}$ have been shifted to coincide with the experimental intensities of the highest peak in the range $J_{CO} \in [35–55]$.
[53] See Supplemental Material at http://link.aps.org/supplemental/10.1103/PhysRevLett.118.253001, which includes Refs. [54,55], for a brief description of the experimental and computational work.
[54] M. L. Lipciuc, A. J. van den Brom, L. Dinu, and M. H. M. Janssen, Rev. Sci. Instrum. **76**, 123103 (2005).
[55] J. A. Schmidt, M. S. Johnson, U. Lorenz, G. C. McBane, and R. Schinke, J. Chem. Phys. **135**, 024311 (2011).